New insights into kinetics and thermodynamics of interfacial polymerization

S. K. Karode,*† S. S. Kulkarni,* A. K. Suresh‡ and R. A. Mashelkar§¶

*Polymer Science and Engineering Group, Chemical Engineering Division, National Chemical Laboratory, Pune 411 008, India; ‡Department of Chemical Engineering, Indian Institute of Technology, Powai, Mumbai 400 076, India; §Council of Scientific and Industrial Research, New Delhi 110 001, India

Abstract—A comprehensive model is developed for interfacial polymerization (IP), which provides new insights into the kinetics of film formation, the molecular weight distribution of the polymer as well as the mechanism of polymer precipitation. We incorporate a more general reaction scheme as well as polymer phase separation both by nucleation of the polymer-rich phase as well as by spinodal decomposition. The model predictions are verified against experimental data for unstirred Nylon 6–10 system. The model predicts that spinodal decomposition is the dominant mechanism of polymer phase separation at short reaction times. Film growth by nucleation of the polymer-rich phase dominates at larger times. The model also predicts the dominance of the nucleation mode of film growth with dilution of the organic phase. This model provides a further step towards a rational design and prediction of properties of membranes/capsules produced by interfacial polymerization.

Keywords: Interfacial polymerization; nylon 6–10; kinetics; thermodynamics; nucleation; spinodal decomposition.

1. INTRODUCTION

Interfacial polymerization (IP) involves step polymerization of two highly reactive monomers, each dissolved in two immiscible phases (Morgan and Kwolek, 1959). The relative ease of IP has made it the preferred technique for forming reverse osmosis membranes (Petersen, 1993) and encapsulation of inks, insecticides or drugs (Khilar, 1987). It is known that the IP conditions affect properties such as the molecular weight of the polymer (Morgan and Kwolek, 1959; Johnson, 1985), the permeability of the deposited thin film in composite membranes (Cadotte *et al*., 1981), etc.

Inspite of extensive experimental and modeling efforts spanning close to four decades, one is still not able to *a priori* to predict the polymer film properties given the physicochemical and thermodynamic parameters of the system. In most of the previous modeling efforts (see Karode *et al*., 1997), the primary aim was to predict the growth rate of the polymer film with reaction time in terms of the diffusion and reaction rate constants. Recently, we have taken a step towards predicting polymer characteristics, starting with estimation of the molecular weight distribution (Karode *et al*., 1997). Such a predictive capability is essential since the molecular weight of the polymer film and its distribution affect a number of polymer characteristics such as mechanical properties, solubility, viscosity and processibility.

It is known that film microstructure and consequent properties such as film density and permeability are affected by the polymer precipitation mechanism (Cheng *et al*., 1995). Therefore, clear insights into the polymer precipitation mechanism are essential. Towards this goal, we launched a modeling effort. In the first such effort (Karode *et al*., 1997), we allowed for polymer phase separation only via spinodal decomposition. The possibility of phase separation via the nucleation and growth mechanism was ignored in this model. In this work, we have taken a step forward by incorporating (i) a more general reaction scheme for the growing polymer chain and (ii) polymer phase separation by nucleation of the polymer-rich species. In this more general scheme all three types of growing chains, i.e. amine ended, acid chloride ended and amine-acid chloride ended are specifically accounted for.

The various aspects of this model have been verified against experimental data in the literature for the

Nylon 6–10 system (Johnson, 1985). The model prediction of the film growth rate is shown to be in good agreement with the experimental data of Johnson (1985). The experimentally observed maximum with variation of the organic phase monomer is also effectively picked up by this model. The model predicts that initially the polymer phase separates via spinodal decomposition. Film growth by nucleation of polymer-rich phase dominates at longer reaction times. Also, film growth by nucleation dominates as the organic phase concentration decreases.

2. AN IMPROVED MODEL FOR FILM FORMATION BY IP

The schematic of film formation via IP is shown in Fig. 1. The reaction scheme now considers all the possible end-capped oligomers as well as polymer precipitation by nucleation.

2.1. *Model development with generalized reaction scheme*

The nomenclature for monomer and polymeric species along with the general reaction scheme is given in Table 1. Several assumptions have been made in the model development. The reaction is assumed to occur in a thin layer in the organic phase adjacent to the interface represented by ε in Fig. 1. The rate of movement of the polymer film–organic phase interface due to polymer formation is assumed to be small in comparison to the rate of diffusion of A_0, so that a pseudo-steady-state approximation can be considered valid for the diffusion of A_0 through the polymer film (see Yadav *et al.*, 1990). The product of reaction (HCl) is assumed to rapidly diffuse to the aqueous phase, where it is neutralized by the acid acceptor. HCl mass balance in the reaction zone, based on that produced by the polymerization reaction and that which diffuses back to the aqueous phase, shows that the HCl concentration is negligible compared to the organic acid chloride concentration. Protonation of the aqueous amine is assumed to be negligible due to an excess of acid acceptor. The rate constant k is the rate constant for reaction between one $-NH_2$ group and one $-COCl$ group. The usual equal reactivity hypothesis is assumed while writing the rate expressions for the reactions in Table 1.

We define the following non-dimensional variables:

$$A^*_{0a} = \frac{A^0_{0a} - A_{0a}}{A_{0a}}, \quad A^*_{mr} = \frac{A_{mr}}{B^0_{0s}}, \quad B^*_{0s} = \frac{B_{0s}}{B^*_{0s}},$$

$$B^*_{mr} = \frac{B_{mr}}{B^0_{0s}}, \quad C^*_{mr} = \frac{C_{mr}}{B^0_{0s}}, \quad \tau = k_i B^0_{0s} t. \tag{1}$$

The governing equations for the concentration of A_0 and B_0 in bulk aqueous and organic phases, respectively, is given by

$$\frac{dA^*_{0a}}{d\tau} = \left(\frac{k_{LA_0,\text{eff}}\hat{a}_I}{k_i B^0_{0s}}\right) \times \left\{1 - A^*_{0a} - \frac{K_{A_0,ps}}{K_{A_0,ap}} \frac{B^0_{0s}}{A^0_{0a}} A^*_{0r}\right\} \tag{2}$$

$$\frac{dB^*_{0s}}{d\tau} = -\left(\frac{k_{LB_0}\hat{a}_I}{k_i B^0_{0s}} \frac{V_a}{V_s}\right)(B^*_{0s} - B^*_{0r}) \tag{3}$$

where

$$k_{LA_0,\text{eff}} = \frac{k_{LA_0}}{\left(1 + \dfrac{k_{LA_0}\delta_t}{K_{A_0,ap} D_{A_0}}\right)}$$

is the effective mass transfer coefficient for transport of A_0 from the bulk aqueous phase into the reaction zone.

The governing equations of the monomers in the reaction zone are given by

$$\frac{dA^*_{0r}}{d\tau} = \left(\frac{k_{LA_0,\text{eff}}}{k_i B^0_{0s}\varepsilon}\right)\left\{\left(\frac{A^0_{0a}}{B^0_{0s}}\right)(1 - A^*_{0a}) - \frac{K_{A_0,ps}}{K_{A_0,ap}} A^*_{0r}\right\} - A^*_{0r}\left\{B^*_{0r} + \left(\frac{k_{p1}}{k_i}\right)(S^*_{B\infty} - B^*_{0r}) + \left(\frac{k_{p2}}{k_i}\right) S^*_{C\infty}\right\} \tag{4}$$

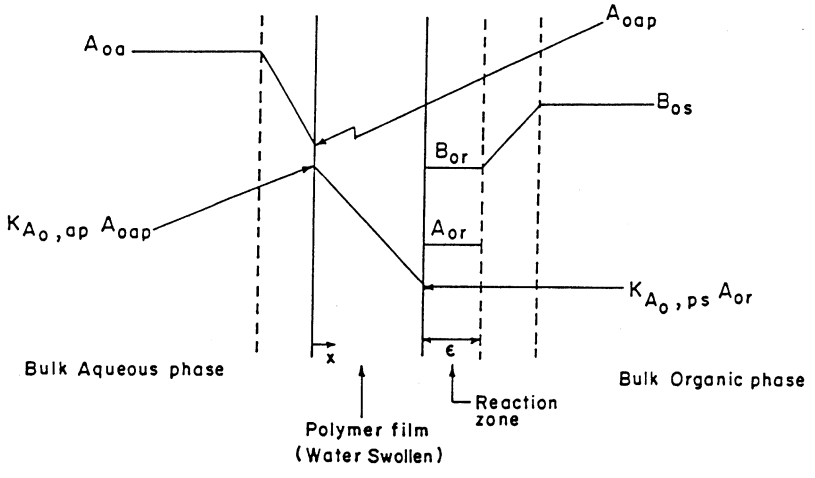

Fig. 1. Schematic of polymer film formation by interfacial polycondensation.

Table 1. General reaction scheme for Nylon 6–10 IP

Symbol	Represents
A_0	$H_2N–R_1–NH_2$ (Monomer-I)
B_0	$ClOC–R_2–COCl$ (Monomer II)
C_0	H–Cl
A_n	$H–(NH–R_1–NHCO–R_2–CO)_n–NH–R_1–NH_2$
B_n	$Cl–(OC–R_2–CONH–R_1–NH)_n–OC–R_2–COCl$
C_n	$H–(NH–R_1–NHCO–R_2–CO)_n–Cl$

Reaction	Index range	Rate
Initiation		
$A_0 + B_0 \rightarrow C_1 + C_0$		$k_i A_0 B_0$
Propagation		
$A_m + B_n \rightarrow C_{m+n+1} + C_0$	$m \neq n$; $m \geqslant 0$, $n \geqslant 0$	$k_{p1} A_m B_n$
$A_n + C_m \rightarrow A_{m+n} + C_0$	$m \geqslant 1$; $n \geqslant 0$	$k_{p2} A_n C_m$
$B_n + C_m \rightarrow B_{m+n} + C_0$	$m \geqslant 1$; $n \geqslant 0$	$k_{p3} B_n C_m$
$C_m + C_n \rightarrow C_{m+n} + C_0$	$n, m \geqslant 1$	$k_{p4} C_m C_n$

$$\frac{dB^*_{0r}}{d\tau} = \left(\frac{k_{LB_0}}{k_i B^0_{0s}\varepsilon}\right)(B^*_{0s} - B^*_{0r}) - B^*_{0r}\left\{A^*_{0r} + \left(\frac{k_{p1}}{k_i}\right)(S^*_{A\infty} - A^*_{0r}) + \left(\frac{k_{p3}}{k_i}\right)S^*_{C\infty}\right\}. \quad (5)$$

The governing equation for the reaction product (C_{0r}) is given by

$$\frac{dC^*_{0r}}{d\tau} = 0 \quad (6)$$

since it is assumed that the reaction product is instantaneously neutralized by the acid acceptor added to the aqueous phase.

The governing equations for the oligomers (chain length $m \geqslant 1$) in the reaction zone are given by

$$\frac{dA^*_{mr}}{d\tau} = -A^*_{mr}\left\{\left(\frac{k_{p1}}{k_i}\right)S^*_{B\infty} + \left(\frac{k_{p2}}{k_i}\right)S^*_{C\infty}\right\} + \left(\frac{k_{p2}}{k_i}\right)\sum_{n=1}^{m} A^*_{(m-n)r}C^*_{nr} \quad (7)$$

$$\frac{dB^*_{mr}}{d\tau} = -B^*_{mr}\left\{\left(\frac{k_{p1}}{k_i}\right)S^*_{A\infty} + \left(\frac{k_{p3}}{k_i}\right)S^*_{C\infty}\right\} + \left(\frac{k_{p3}}{k_i}\right)\sum_{n=1}^{m} B^*_{(m-n)r}C^*_{nr} \quad (8)$$

$$\frac{dC^*_{mr}}{d\tau} = -C^*_{mr}\left\{\left(\frac{k_{p2}}{k_i}\right)S^*_{A\infty} + \left(\frac{k_{p3}}{k_i}\right)S^*_{B\infty}\right\} + \left(\frac{k_{p1}}{k_i}\right)\sum_{n=1}^{m} A^*_{(m-n)r}B^*_{(n-1)r} + A^*_{0r}B^*_{0r}\delta_{m1} - \left(\frac{k_{p4}}{k_i}\right)C^*_{mr}S^*_{C\infty} + \left(\frac{k_{p4}}{k_i}\right)\sum_{n=1}^{m-1} C^*_{nr}C^*_{(m-n)r}. \quad (9)$$

In the model development so far, the reaction rates of the initiation and propagation reactions can be calculated using the equal reactivity hypothesis as $k_i = 4k$, $k_{p1} = 4k$, $k_{p2} = 2k$ and $k_{p4} = k$.

The governing equation for $S^*_{A\infty}$ ($\sum_{n=0}^{\infty} A^*_{nr}$) in the reaction zone can be written by summing eq. (7) from $n = 1$ to $n = \infty$ and adding eq. (4). This is given by

$$\frac{dS^*_{A\infty}}{d\tau} = \left(\frac{k_{LA_0,\mathrm{eff}}}{k_i B^0_{0s}\varepsilon}\right)\left\{\left(\frac{A^0_{0a}}{B^0_{0s}}\right)(1 - A^*_{0a}) - \frac{K_{A_0,ps}}{K_{A_0,ap}}A^*_{0r}\right\} - A^*_{0r}\left\{B^*_{0r} + \left(\frac{k_{p1}}{k_i}\right)(S^*_{B\infty} - B^*_{0r}) + \left(\frac{k_{p2}}{k_i}\right)S^*_{C\infty}\right\} - (S^*_{A\infty} - A^*_{0r})\left\{\left(\frac{k_{p1}}{k_i}\right)S^*_{B\infty} + \left(\frac{k_{p2}}{k_i}\right)S^*_{C\infty}\right\} + \left(\frac{k_{p2}}{k_i}\right)S^*_{A\infty}S^*_{C\infty}. \quad (10)$$

Similarly governing equations can be written for $S^*_{B\infty}$ and $S^*_{C\infty}$ as

$$\frac{dS^*_{B\infty}}{d\tau} = \left(\frac{k_{LB_0}}{k_i B^0_{0s}\varepsilon}\right)(B^*_{0s} - B^*_{0r}) - B^*_{0r}\left\{A^*_{0r} + \left(\frac{k_{p1}}{k_i}\right)(S^*_{A\infty} - A^*_{0r}) + \left(\frac{k_{p3}}{k_i}\right)S^*_{C\infty}\right\} - (S^*_{B\infty} - B^*_{0r})\left\{\left(\frac{k_{p1}}{k_i}\right)S^*_{A\infty} + \left(\frac{k_{p3}}{k_i}\right)S^*_{C\infty}\right\} + \left(\frac{k_{p3}}{k_i}\right)S^*_{B\infty}S^*_{C\infty} \quad (11)$$

$$\frac{dS^*_{C\infty}}{d\tau} = A^*_{0r}B^*_{0r} + \left(\frac{k_{p1}}{k_i}\right)S^*_{B\infty}(S^*_{A\infty} - A^*_{0r}) + \left(\frac{k_{p2}}{k_i}\right)S^*_{A\infty}S^*_{C\infty} + \left(\frac{k_{p3}}{k_i}\right)S^*_{B\infty}S^*_{C\infty} - S^*_{C\infty}\left\{\left(\frac{k_{p2}}{k_i}\right)S^*_{A\infty} + \left(\frac{k_{p3}}{k_i}\right)S^*_{B\infty}\right\} + \left(\frac{k_{p1}}{k_i}\right)S^*_{A\infty}S^*_{B\infty} + \left(\frac{k_{p4}}{k_i}\right)S^*_{C\infty}S^*_{C\infty}. \quad (12)$$

Defining $P^*_{mr}(=A^*_{mr}+B^*_{mr}+C^*_{mr})$ as the total non-dimensional concentration of species of chain length m within the reaction zone, the governing equation for P^*_{mr} can easily be written as:

$$\frac{dP^*_{mr}}{d\tau}=\frac{dA^*_{mr}}{d\tau}+\frac{dB^*_{mr}}{d\tau}+\frac{dC^*_{mr}}{d\tau} \tag{13}$$

The initial conditions for the above set of equations are

$$A^*_{0a}=0,\ A^*_{mr}=0,\ B^*_{0r}=1,$$
$$B^*_{mr}=0\ m>0,\ C^*_{mr}=0,\ B^*_{0s}=1. \tag{14}$$

The initial conditions for $S^*_{A\infty}$, etc., can be derived from eq. (14).

2.2. *Polymer precipitation by nucleation*

Two mechanisms for polymer phase separation are considered in this work: nucleation of polymer-rich phase and spinodal decomposition. Growth of the nucleated particles is neglected as being of secondary importance.

Nucleation of polymer primary particles based on the thermodynamics of phase equilibrium of monodispersed polymer/single solvent has been modeled by Kamide *et al.* (1993). The formation of polymer primary particles by nucleation is considered to be substantially similar to the condensation of liquid droplets from super-saturated vapors or the formation of ice particles from supercooled liquids.

The free energy change of coagulation per unit volume (Δf_v) is given by

$$\Delta f_v=\Delta\bar{G}(\phi_m)-\Delta G_v(\phi_m) \tag{15}$$

where $\Delta\bar{G}$ is the average Gibbs' free energy of coexisting (phase separated) phases and ΔG_v is the Gibbs' free energy change of mixing per unit volume. ϕ_m is the volume fraction of oligomeric species of chain length m (i.e. P_{mr} species). $\Delta\bar{G}$ is defined as

$$\Delta\bar{G}(\phi_m)=\frac{\Delta G_v(\phi^U_m)-\Delta G_v(\phi^L_m)}{\phi^U_m-\phi^L_m}(\phi_m-\phi^L_m)+\Delta G_v(\phi^L_m). \tag{16}$$

ΔG_v is calculated as

$$\Delta G_v(\phi_m)=(1-\phi_m)\left(\frac{\Delta\mu_s}{v_s}\right)+\phi_m\left(\frac{\Delta\mu_m}{mv_s}\right). \tag{17}$$

Here, $\Delta\mu_s$ and $\Delta\mu_m$ are the chemical potentials of the solvent and P_{mr} species, respectively. The chemical potentials are calculated from Flory–Huggins' theory (Flory, 1953). v_s is the molar volume of the solvent, and ϕ^U_m and ϕ^L_m are, respectively, the volume fractions of P_{mr} species at the upper branch of the binodal and the lower branch of the binodal (calculated from Flory-Huggins' theory) at the temperature of phase separation.

The volume fraction of the oligomer of chain length m can be calculated from the non-dimensional concentration P^*_{mr} as follows:

$$\phi_m=\frac{M_m P^*_{mr} B^0_{0s}}{\rho_p} \tag{18}$$

where M_m is the molecular weight of P_{mr} species (taken as the average of A_{mr}, B_{mr} and C_{mr}) and ρ_p is the density of the polymer. The density of the oligomer is assumed to be the same as that of the polymer.

The critical radius of the spherical nucleus of P_{mr} species which phase-separates from a bulk solution with oligomer volume fraction ϕ_m is given by

$$R_{CN,m}=-2\sigma/\Delta f_v. \tag{19}$$

where σ is the interfacial energy between the nucleus and the surrounding lean phase. This can be estimated from contact angle data as suggested by Fowkes (1964) and Owens and Wendt (1969) assuming that the polymer-lean phase consists essentially of pure solvent.

2.2.1. *Rate of nucleation.*

The rate of nucleation of oligomeric species of length m is assumed to be proportional to the excess of that species with respect to the lower branch of the binodal. The volumetric rate of nucleation of P_{mr} species is assumed to be given by the following phenomenological relationship (see Gonzalez-Ortiz and Asua, 1996):

$$\frac{dV_m}{dt}=k_m(\phi_m-\phi^L_m) \tag{20}$$

where k_m is the phenomenological rate constant of nucleation in units of m^3/s.

Accounting for the rate of nucleation, the governing equation for P^*_{mr} [eq. (13)] changes as follows:

$$\frac{dP^*_{mr}}{d\tau}=\frac{d}{d\tau}(A^*_{mr}+B^*_{mr}+C^*_{mr})-\left(\frac{1}{a\varepsilon}\right)\left(\frac{\phi^U_m\rho_p}{B^0_{0s}M_m}\right)\frac{dV_m}{d\tau} \tag{21}$$

where $dA^*_{mr}/d\tau$, $dB^*_{mr}/d\tau$ and $dC^*_{mr}/d\tau$ are calculated from eqs (7)–(9).

The second term in the above equation appears because of the consumption of the P^*_{mr} species due to nucleation, leading to non-reactive nuclei. This had been ignored in our earlier model (Karode *et al.*, 1997).

2.2.2. *Condition for formation of a coherent film.*

Once the polymer-rich primary particles are formed via nucleation, they would coalesce to form a coherent polymer film. In the nucleation mode, it is assumed that a coherent film will form when the projected area of all the phase-separated nuclei equals the interfacial area for reaction (a). It is further assumed that the number fraction of nuclei of any chain length in the polymer film is the same as the fractional concentration of that chain length species in the reaction volume.

The fraction of oligomeric species of chain length m in the reaction zone is given by $P^*_{mr}/\sum_{n=0}^{\infty}P^*_{nr}$. A coherent polymer film would form if the following

inequality is satisfied (projected area criterion):

$$\sum_{m=0}^{\infty}\left\{\left(\frac{P^*_{mr}}{\sum_{n=0}^{\infty}P^*_{nr}}\right)N_{CN,m}\pi R^2_{CN,m}\right\}\geqslant a \qquad (22)$$

where $N_{CN,m}$ is the number of critical nuclei of species of chain length m. This can be calculated from $R_{CN,m}$ and dV_m assuming nuclei to be spherical in shape.

Once the above inequality is satisfied, the thickness of the polymer film can be calculated (from a mass balance) as follows:

$$\delta' = \left(\frac{1}{a\rho_f}\right)\sum_{m=0}^{\infty}\left\{\left(\frac{P^*_{mr}}{\sum_{n=0}^{\infty}P^*_{nr}}\right)N_{CN,m}\frac{4}{3}\pi R^3_{CN,m}\phi^U_m\rho_p\right\} \qquad (23)$$

where ρ_f and ρ_p are the densities of the polymer film and of the polymer, respectively.

2.3. *Polymer precipitation by spinodal decomposition*

If the concentration of P^*_{mr} exceeds the concentration of the lower branch of the spinodal (Flory, 1953), the polymer film is assumed to form due to instantaneous precipitation via spinodal decomposition. The procedure for estimating the molecular weight distribution of the polymer precipitated by this mode in the film is the same as that given in the earlier model (Karode *et al*., 1997). In the extended model, both spinodal decomposition and nucleation modes can co-exist. The increase in total film thickness is obtained by summing the contribution to the growth of film thickness by nucleation using eq. (23) and that by spinodal decomposition using eq. (25) of the earlier model (Karode *et al*., 1997).

The polymer film growth by spinodal decomposition is handled numerically as detailed in our earlier work (Karode *et al*., 1997). Film growth by nucleation occurs only when eq. (22) is satisfied. The increase in film thickness due to nucleation is calculated by eq. (23).

2.4. *Solution strategy*

Equations (7)–(9) form an infinite set of first-order ODEs representing the governing equations for oligomers of various chain lengths. In this study, the maximum oligomer chain length was set to 100. This limit was chosen as our earlier study (Karode *et al*., 1997) indicated that the average chain length in the Nylon 6–10 system was <80 and that the number fraction of oligomers with chain length more than 95 was less than 0.01. Hence, the resulting 305 first-order ODEs [eqs (2)–(13)] were simultaneously integrated by the fourth-order Runge–Kutta method (Press *et al*., 1990).

The instantaneous number and weight-average molecular weight of the polymer film can be calculated as

$$M_{pN} = \frac{\sum_m\left\{\left(\frac{P^*_{mr}}{\sum_m P^*_{mr}}\right)N_{CN,m}\frac{4}{3}\pi R^3_{CN,m}\phi^U_m\frac{\rho_p}{M_m}M_m\right\}}{\sum_m\left\{\left(\frac{P^*_{mr}}{\sum_m P^*_{mr}}\right)N_{CN,m}\frac{4}{3}\pi R^3_{CN,m}\phi^U_m\frac{\rho_p}{M_m}\right\}} \qquad (24)$$

and

$$M_{pW} = \frac{\sum_m\left\{\left(\frac{P^*_{mr}}{\sum_m P^*_{mr}}\right)N_{CN,m}\frac{4}{3}\pi R^3_{CN,m}\phi^U_m\frac{\rho_p}{M_m}M_m\right\}}{\sum_m\left\{\left(\frac{P^*_{mr}}{\sum_m P^*_{mr}}\right)N_{CN,m}\frac{4}{3}\pi R^3_{CN,m}\phi^U_m\frac{\rho_p}{M_m}M_m\right\}} \qquad (25)$$

The time-averaged molecular weights $\bar{M}_{pN}$ and $\bar{M}_{pW}$ represent the average molecular weight of the polymer film precipitated upto time t. These can be calculated by keeping track of all the polymeric species which undergo phase separation and form the coherent polymer film. The polydispersity of the polymer film is calculated as the ratio of $\bar{M}_{pW}$ and $\bar{M}_{pN}$.

2.5. *Estimation of model parameters*

The molecular weight and distribution of the interfacially polymerized polymer film was found to depend on the relative rate of reaction (k) compared to the rate of nucleation (k_m) (Karode, 1997). Hence, these were used as adjustable parameters to fit the model to experimental data (Johnson, 1985) on the polymer film growth rate for one solvent.

The value of the reaction rate constant k has been indicated to be in the range 10^2 to 10^4 kmol/m^3 s (Morgan, 1965). The value of k found by fitting the experimental data is within this range. The nucleation model (Kamide *et al*., 1993) requires parameters which cannot be determined for our system and hence an *a priori* estimate of the rate constant of nucleation k_m was not possible. Gonzalez-Ortiz and Asua (1996) have also treated k_m as an adjustable model parameter for determining the nucleation rate. The other model parameters are given in Table 2. The methods used for estimating these parameters are reported in our earlier work (Karode *et al*., 1997).

3. EXPERIMENTAL

The IP film growth rate data used by us was reported by Johnson (1985). Johnson's experiment was repeated by us to measure the crystallinity of the polymer film. Methylene chloride (MC) was used as the organic solvent and the experiment was done at two acid phase concentrations 0.13 and 0.065 kmol/m^3. The amine concentration was 0.4 kmol/m^3. The reaction was allowed to continue for 200 s before it was stopped by adding HCl. The polymer film was washed with water and dried. The intrinsic viscosities of the film in concentrated H_2SO_4 were found to be in good agreement with the values reported by Johnson (1985). Wide-angle X-ray diffraction spectra were measured on a Phillips PW 1730 model with a CuK_α beam. The spectra in the 2θ range from 14 to 28° were deconvoluted to estimate the crystalline fraction.

4. RESULTS AND DISCUSSION

Johnson (1985) has reported data on the polymer film thickness as a function of reaction time for the unstirred Nylon 6-10 polymerization. Three organic

Table 2. Parameter values for application of the model to experimental data

Parameter	Value
a	40×10^{-4} (m^2)*
k	7×10^2 (kmol/m^3 s)
k_m	2.5×10^{-10} m^3/s
$k_{L_{A0}}$, $k_{L_{B0}}$	10^{-7} (m/s)†
D_{A0}	3×10^{-11} (m^2/s)†
ε_r	10^{-8} m†
ρ_f	200 (kg/m^3)*
ρ_p	1090 (kg/m^3)‡
σ	4.86×10^{-3} J/m^2§

Solvent	Interaction parameter‡	Partition coefficient*
MC	1.33	1.25
DCE	2.29	3.0
CFM	1.74	0.7

*Johnson (1985).
†Karode *et al.* (1997).
‡Brandrup and Immergut (1989).
§Owens and Wendt (1969).

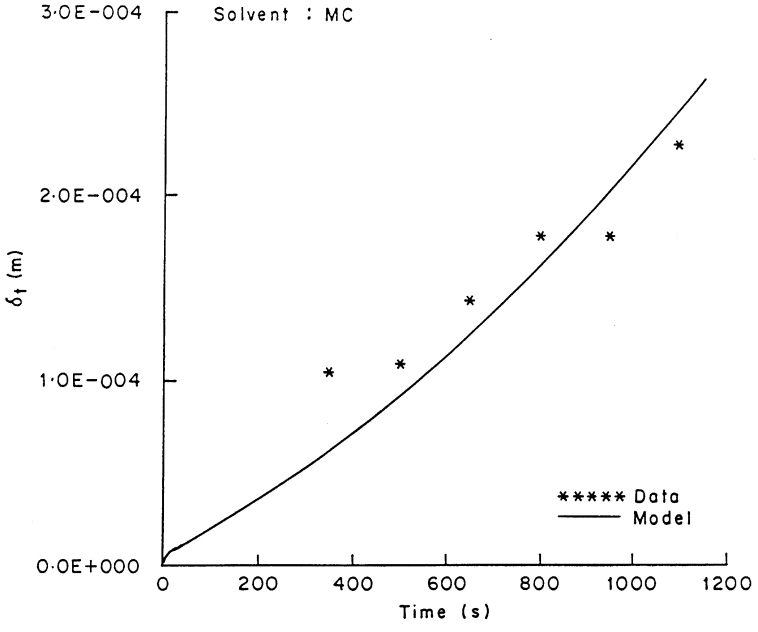

Fig. 2. Polymer film thickness as a function of reaction time in MC. Experimental data (Johnson, 1985) and model prediction at $B_{0s}^0 = 0.13$ kmol/m^3 using parameters in Table 2.

solvents were used: methylene chloride (MC), chloroform (CFM) and dichloroethane (DCE). The variation of film intrinsic viscosity (at 200 s reaction time) with organic phase concentration was also studied. The model developed was fitted to the film thickness–time experimental data at one set of reagent conditions with MC as solvent by varying k and k_m and using the parameters listed in Table 2. These parameters were then used to predict the film thickness, molecular weight and polydispersity of the polymer film in the other two solvents by substituting the appropriate values of χ and $K_{A0,ps}$. These molecular weight predictions are compared with the data on the intrinsic viscosity of the polymer film as a function of organic-phase concentration reported by Johnson (1985). The model is also used to predict the mode of polymer precipitation at various IP conditions.

4.1. *Film thickness vs reaction time*

Figures 2–4 show the model prediction of polymer film thickness as a function of reaction time for organic solvents MC, CFM and DCE, respectively. The model parameters (k and k_m) were estimated by fitting the model predictions to MC data. When these values were used to predict the film thickness vs time for the other two solvents, the agreement with experimental

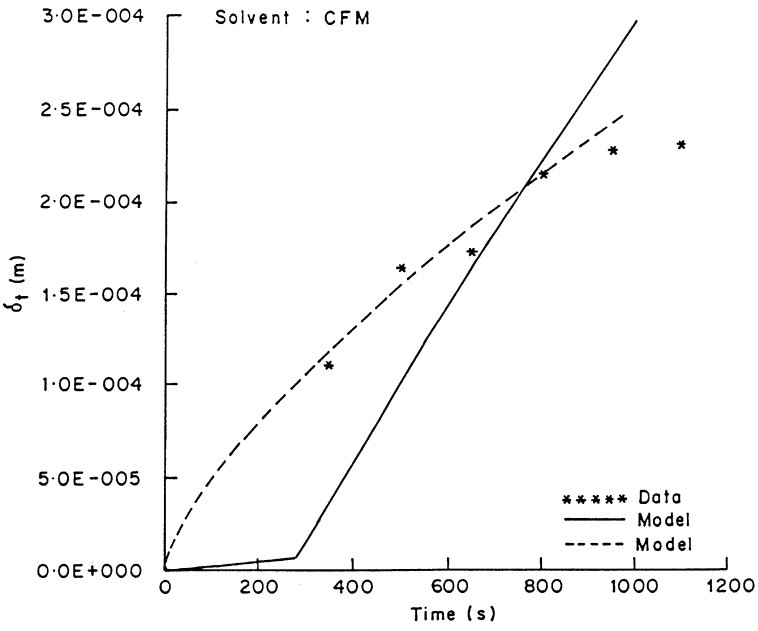

Fig. 3. Polymer film thickness as a function of reaction time in CFM. Experimental data (Johnson, 1985) and model prediction at $B^0_{0s} = 0.18$ kmol/m^3 using parameters in Table 2. Dashed line with $k_m = 3.7 \times 10^{-10}$.

data was not as good. With other solvents, the model appears to underpredict the polymer film thickness at low reaction times. If it is assumed that k_m varies with the type of solvent, a better fit to the data for CFM and DCE can be obtained as shown by *the dashed* lines in Figs 3 and 4. These predictions of δ_t vs time show that the rate of growth is very high at low times (<1 s) and decreases as the polymer film increases in thickness. As shown in Fig. 4(b), most of the polymer precipitates by spinodal decomposition. However, increasing k_m causes a substantial increases in the rate of film growth at low reaction times [see Fig. 4(a)]. Unfortunately, experimental data at low times are not available to enable a more accurate estimation of k_m. These k_m values leading to a better fit of experimental data can be correlated with the interaction parameter (χ). Figure 5 suggests that the nucleation rate constant is higher in poorer solvents.

The effect of the organic phase concentration on the polymer film thickness is shown in Fig. 6 for CFM as a representative solvent. The predictions of this improved model are seen to be in line with the general experimental trends. Unlike the previous simplified model (Karode *et al.*, 1997), which predicted film thickness to be insensitive to B^0_{0s}, this improved model predicts that as the organic monomer concentration is decreased, the thickness of the polymer film generally reduces. This is consistent with experimental observation (Morgan, 1965).

4.2. *Molecular weight of polymer film as a function of organic monomer concentration*

The effect of organic-phase concentration in CFM on the molecular weight of the polymer film formed at various times is shown in Fig. 7. The experimentally observed molecular weight maximum is also predicted by this improved model, as can be seen from Figs 8–10. The improved model predicts the increase in $\bar{M}_{pW}$ at low B^0_{0s} values better than the simplified model which predicted a shallow maximum. The reason for this maxima in molecular weight is the same as discussed in our previous work (Karode *et al.*, 1997).

It can be seen from these figures that as the organic solvent becomes poorer (i.e. χ increases), the polymer molecular weight also reduces (Morgan, 1965). This is because a poor organic solvent cannot hold the growing oligomers in solution for sufficient time to allow a high molecular weight to build up. The growing oligomers phase separate due to nucleation and are rendered unreactive. This results in slower molecular weight build up.

4.3. *Molecular weight of polymer film as a function of k and k_m*

As expected, at any given acid chloride concentration and a constant value of k parametric studies show that the rate of film growth increases with increasing nucleation rate (increasing k_m). Correspondingly the molecular weight of the precipitating polymer is also predicted to decrease with increasing k_m. This trend is summarized in Fig. 11 which shows that higher molecular weight polymer is formed with increasing values of k/k_m. After a certain limit the molecular weight becomes insensitive to this ratio. This explains why the molecular weight prediction was insensitive to the value of k with the earlier simplified model (Karode *et al.*, 1997).

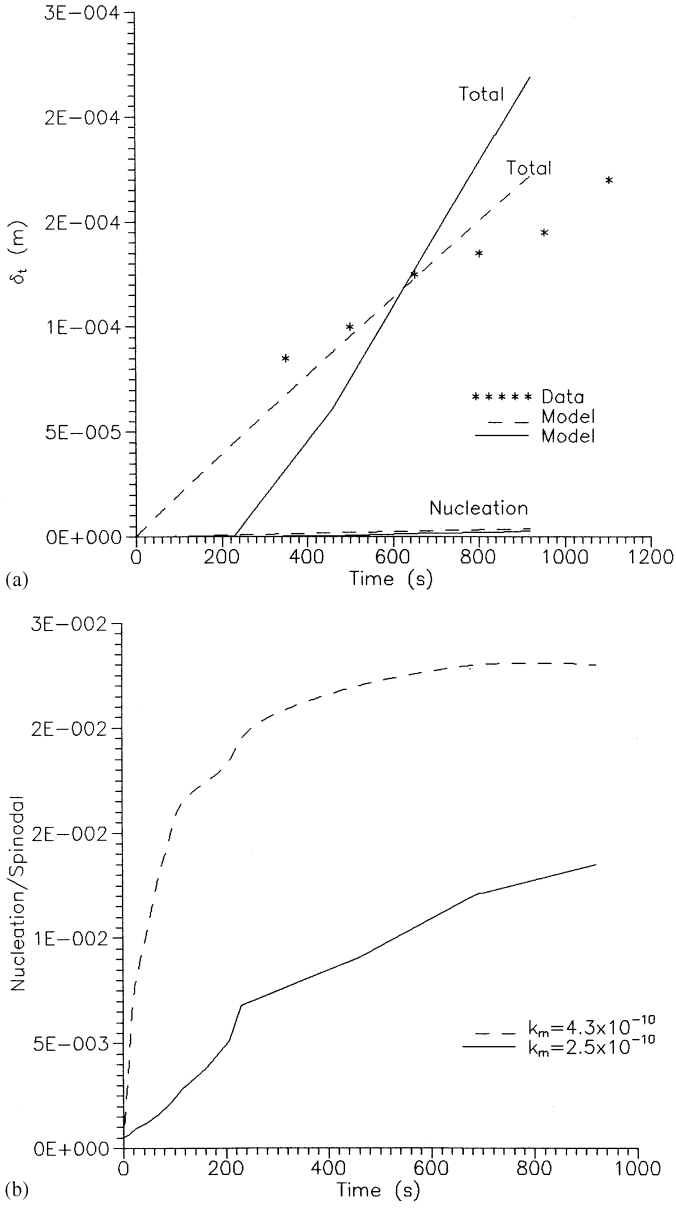

Fig. 4. (a) Polymer film thickness as a function of reaction time in DCE. Experimental data (Johnson, 1985) and model prediction at $B^0_{os} = 0.109\ \text{kmol/m}^3$ using parameters in Table 2. Dashed line with $k_m = 4.3 \times 10^{-10}$. (b) Model prediction of fraction of polymer film precipitated by nucleation to spinodal decomposition at $B^0_{0s} = 0.109\ \text{kmol/m}^3$ using parameters in Table 2. Dashed line with $k_m = 4.3 \times 10^{-10}$.

4.4. *Polymer film characteristics as a function of reaction time*

Figures 12 and 13 show the model prediction of time variation of molecular weight and polydispersity of the oligomers still in solution with CFM as a representative solvent. The oligomer polydispersity decreases with reaction time while its molecular weight increases slowly.

Figure 14 shows that for a dilute organic phase ($B^0_{0s} = 0.01\ \text{kmol/m}^3$), the polydispersity of the polymer film also increases with reaction time. As the organic phase concentration increases, the polymer film polydispersity decreases with reaction time after passing through a maximum. This trend is quite different from the prediction of the earlier model (Karode *et al.*, 1997). The polymer film polydispersity predicted by this improved model is also much higher than that predicted by the earlier model. This is because in the earlier model, it was assumed that precipitation of the polymer film resulted only from spinodal decomposition. Hence, only those species whose concentration was in excess of its spinodal concentration would undergo phase separation. This resulted in a polymer film with relatively less polydispersity. In the present model where nucleation of polymer-rich particles has also been incorporated,

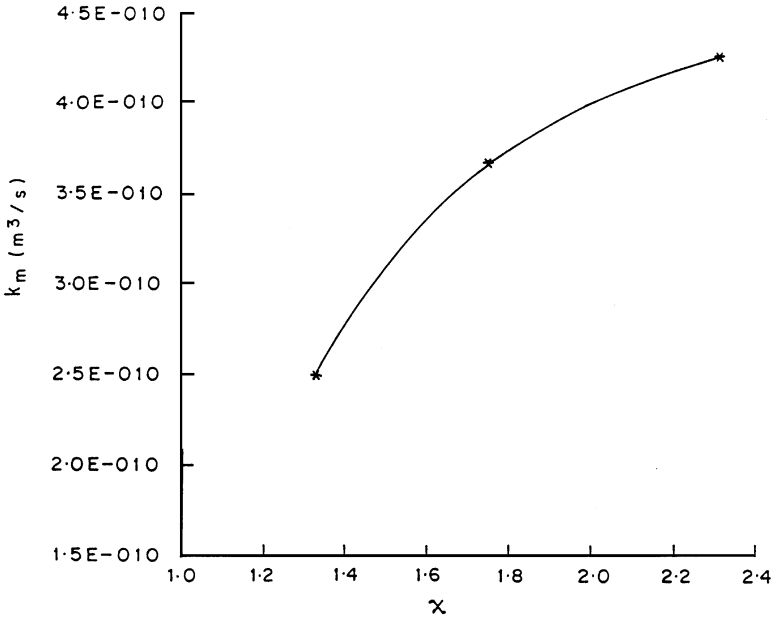

Fig. 5. Variation of k_m with χ.

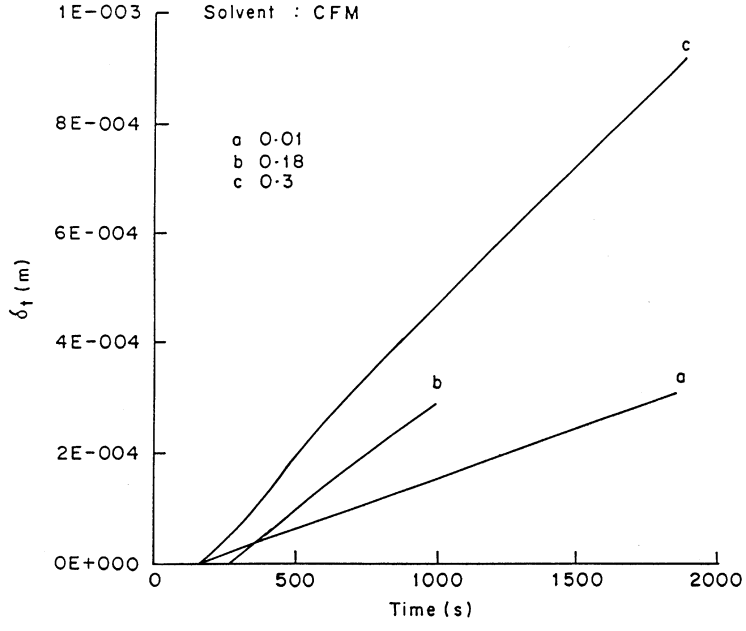

Fig. 6. Model prediction of polymer film thickness versus time for various acid chloride concentrations in CFM using parameters in Table 2.

polymer film formation by nucleation results in a proportional number of nuclei of each chain length being incorporated into the polymer film. This leads to a polymer film which is relatively more polydisperse.

4.5. *Mode of polymer precipitation*

A change in the mode of polymer-phase separation is predicted by the model (see Fig. 3). At low times, the polymer phase separates via spinodal decomposition. Film growth due to nucleation sets in at higher reaction times as seen by the change in slope of the model prediction curve. Since there are no experimental data reported at sufficiently low times, this model prediction cannot be verified.

Figure 15 shows the model prediction of the ratio of the fraction of polymer film formed due to nucleation to the fraction of polymer film formed by spinodal decomposition for various organic phase concentra-

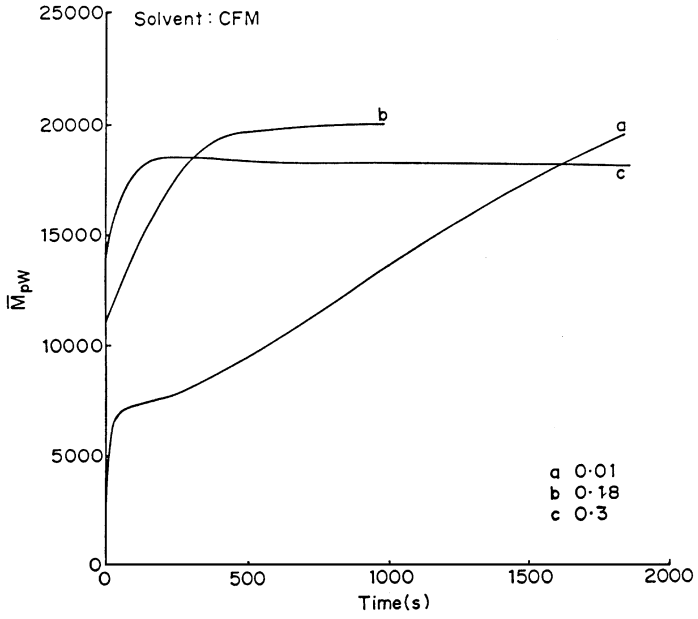

Fig. 7. Model prediction of $\bar{M}_{pW}$ vs reaction time for various acid chloride concentrations in CFM using parameters in Table 2.

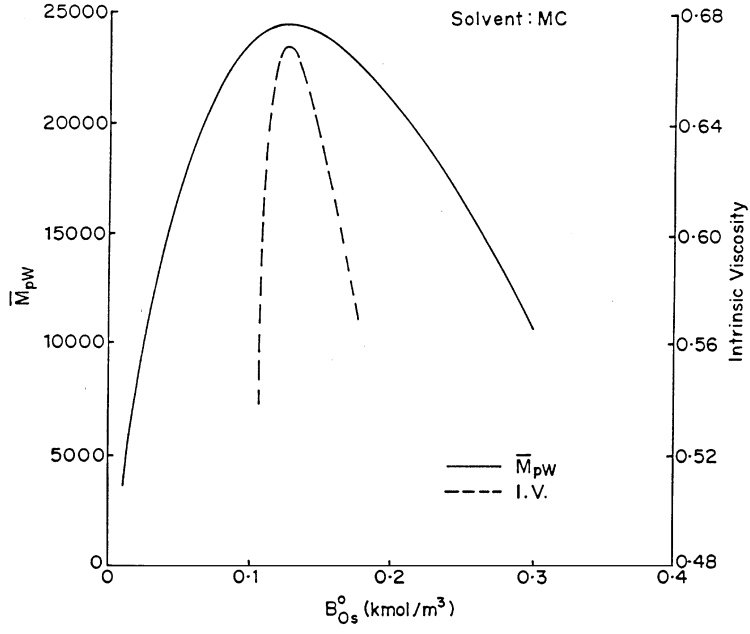

Fig. 8. Model prediction of $\bar{M}_{pW}$ as a function of acid chloride concentration at 200 s in MC. Intrinsic viscosity (measured in concentrated H_2SO_4) data of Johnson (1985).

tion in MC. As can be seen, the polymer film which forms at early reaction times is predominantly formed via spinodal decomposition. Nucleation, being a relatively slow process, becomes more important at large reaction times.

Further, as the organic phase is diluted, the fraction of the polymer film formed via nucleation increases. This model prediction can be indirectly verified by examining the effect of organic-phase concentration on the crystallinity of the IP film. This verification is based on the assumption that nucleation will tend to favor crystalline phase formation more than the faster spinodal decomposition process. It was found that dilution of the organic phase from 0.13 to 0.065 kmol/m^3 resulted in an increase in the crystalline fraction of the polymer film from 0.28 to 0.33.

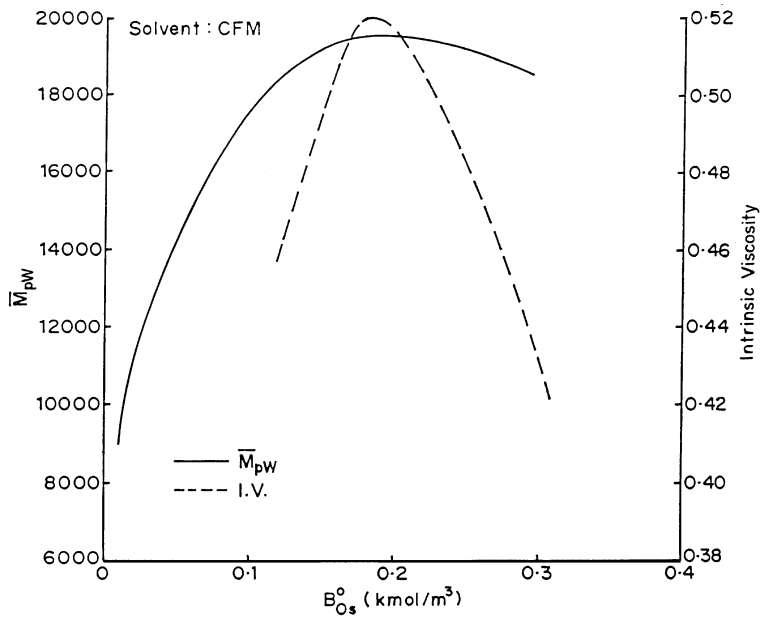

Fig. 9. Model prediction of $\bar{M}_{pW}$ as a function of acid chloride concentration at 200 s in CFM. Intrinsic viscosity (measured in concentrated H_2SO_4) data of Johnson (1985).

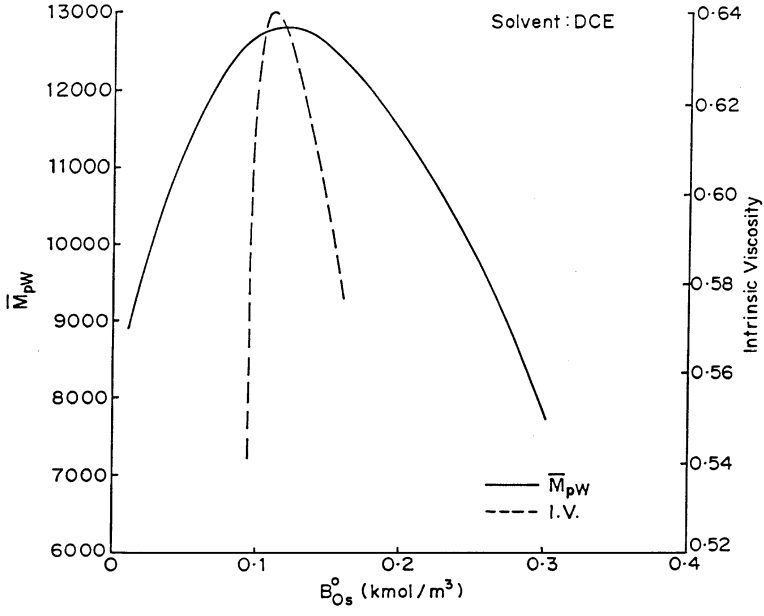

Fig. 10. Model prediction of $\bar{M}_{pW}$ as a function of acid chloride concentration at 200 s in DCE. Intrinsic viscosity (measured in concentrated H_2SO_4) data of Johnson (1985).

Similar experimental data have been reported by Yadav *et al.* (1996) for a polyurea system.

5. CONCLUSIONS

We have developed a comprehensive IP model incorporating a more general reaction scheme as well as polymer phase separation by both nucleation and spinodal decomposition mechanisms. This model is able to fit experimental film growth rate data using two adjustable parameters k and k_m. Unlike the previous model, this improved model predicts the polymer film thickness to be dependent on the organic phase concentration. This is consistent with general experimental trends.

Polymer film characteristics, like its molecular weight and distribution depend on the relative rate of chain growth via chemical reaction compared to the

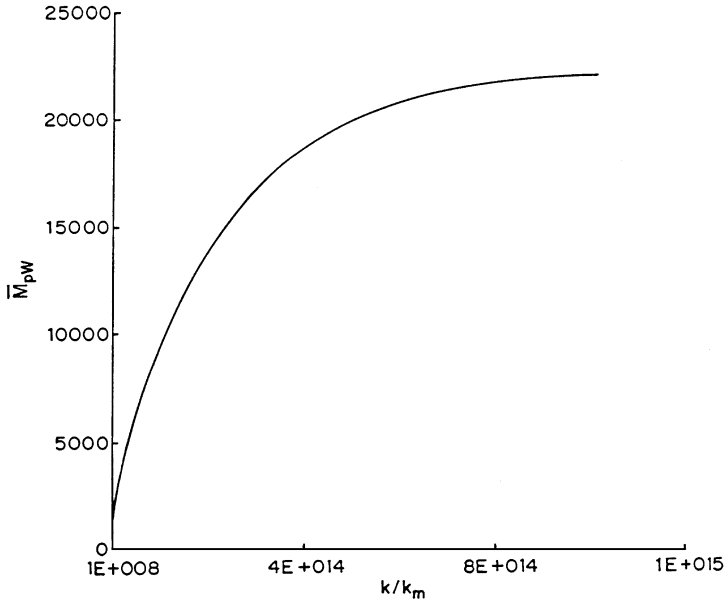

Fig. 11. Model prediction of variation of $\bar{M}_{pW}$ with k/k_m.

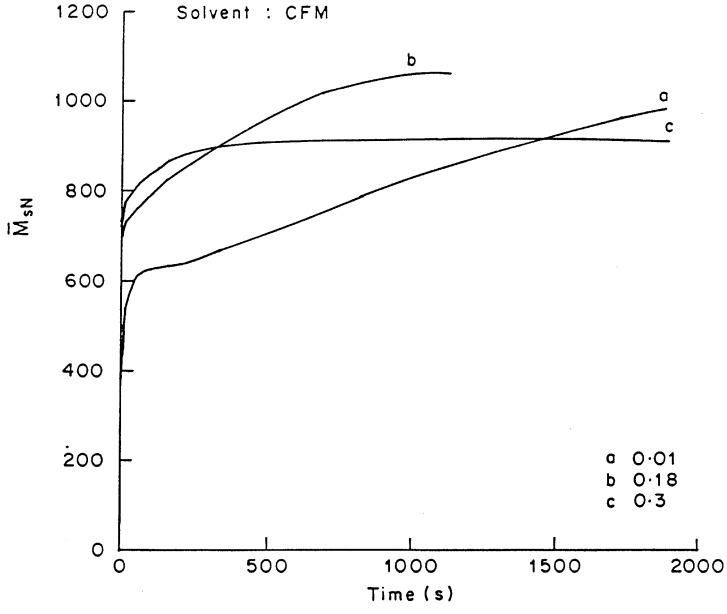

Fig. 12. Model prediction of $\bar{M}_{sN}$ vs reaction time for various acid chloride concentrations in CFM.

rate of phase separation due to nucleation. The higher the reaction rate as compared to the rate of nucleation, higher is the molecular weight of the polymer film.

Literature data are not adequate for determining accurate value(s) of the nucleation rate constant (k_m) for Nylon 6–10 systems. A more accurate estimate of k_m could have been made if film thickness vs time data at short time intervals or on absolute molecular weight data were available. k_m may not be a constant for a particular polymer alone; its value apparently increases for poorer solvents. The molecular weight maximum as a function of organic-phase concentration predicted by the improved model is much sharper than that predicted by the simplified model and agrees better with the intrinsic viscosity data.

Our comprehensive model also predicts polymer film polydispersity to be higher than that predicted by the simplified model. In the previous model, spinodal decomposition was the only operative mode of phase separation; thus, only those species whose concentration was in excess of their spinodal concentration,

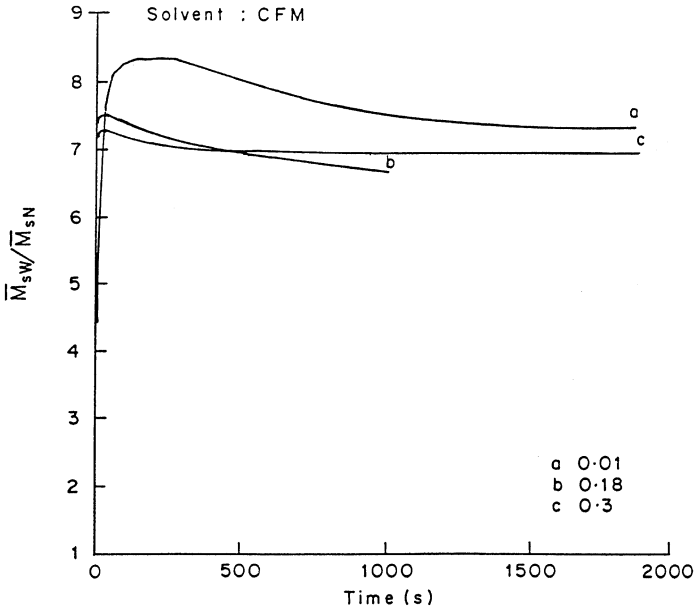

Fig. 13. Model prediction of polydispersity of oligomers in solution vs reaction time for various acid chloride concentrations in CFM.

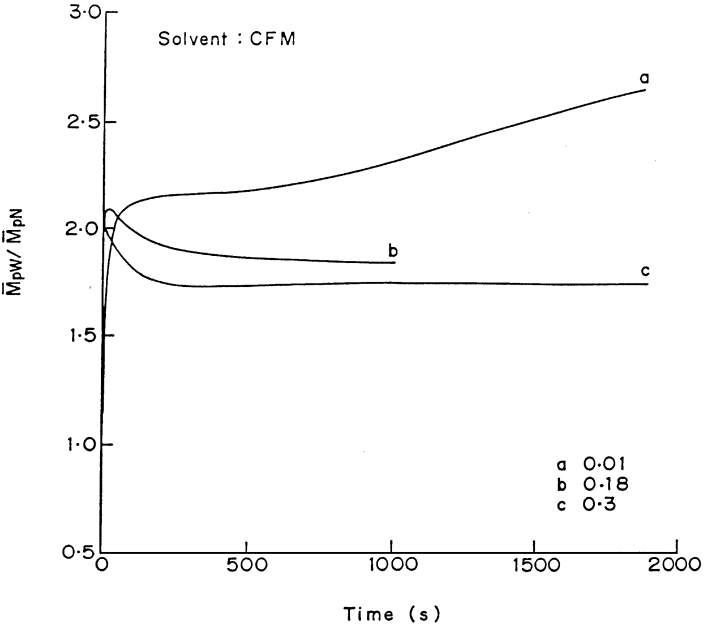

Fig. 14. Model prediction of polydispersity of polymer film vs reaction time for various acid chloride concentrations in CFM.

would phase-separate to form a polymer film. When nucleation is also incorporated in polymer-phase separation, a proportional number of nuclei (of all chain lengths) are incorporated into the growing polymer film, thereby leading to a relatively polydisperse polymer film. The polymer film polydispersities predicted by this improved model are more consistent with experimentally observed values.

The mode of polymer-phase separation can also be predicted by using this comprehensive model. The model predicts spinodal decomposition to be the dominant mode of phase separation at short reaction times. At longer times, phase separation via the nucleation mechanism also becomes significant and the polymer film grows as a result of both mechanisms operating simultaneously. The experimentally

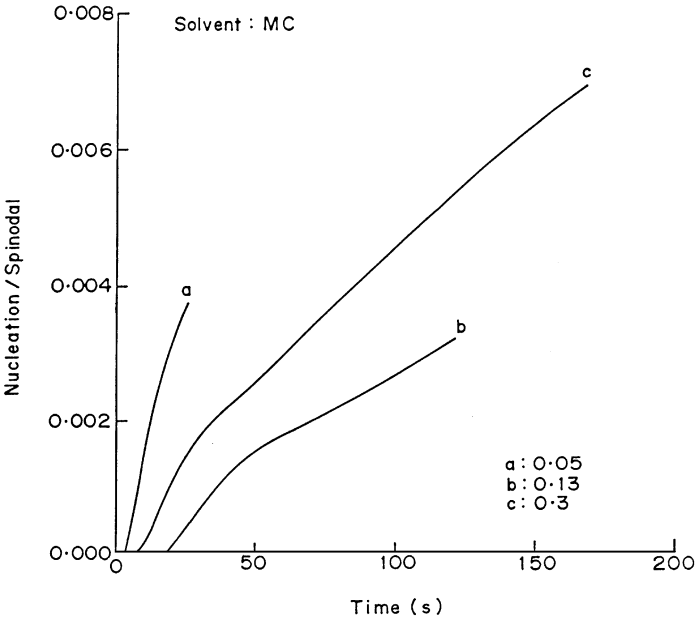

Fig. 15. Predicted of ratio of polymer film precipitated by nucleation and spinodal decomposition mechanisms as a function of time for various acid chloride concentrations in MC.

measured increase in crystallinity with decreasing acid concentration is consistent with the model prediction. This knowledge of the mode of phase separation would eventually be helpful in an *a priori* prediction of the polymer film transport properties. With such an advance, the existing empiricism in the manufacturing of thin polymer films via IP for composite membranes or for drug encapsulation could be reduced.

NOTATION

a interfacial area, m^2

$\hat{a}$ interfacial area per unit aqueous-phase volume, m^{-1}

A_{0a} concentration of aqueous-phase monomer (diamine) in bulk aqueous phase, $kmol/m^3$

A_{0p} concentration of A_0 in the polymer film, $kmol/m^3$

A_{0p} concentration of A_0 in the polymer film, $kmol/m^3$

A_{0r} concentration of A_0 in the reaction zone, $kmol/m^3$

A_{mr} concentration of A_m in the reaction zone, $kmol/m^3$

A_{0ap} concentration of A_0 on aqueous side of aqueous-phase–polymer film interface, $kmol/m^3$

B_{0r} concentration of organic phase monomer (diacid chloride) in the reaction zone, $kmol/m^3$

B_{mr} concentration of B_m species in the reaction zone, $kmol/m^3$

C_{mr} concentration of C_m species in the reaction zone, $kmol/m^3$

D_{A0} diffusion coefficient of A_0 through polymer film, m^2/s

k reaction rate constant between one NH_2 and one COCl group, $m^3/kmol\,s$

k_i reaction rate constant of initiation reaction, $m^3/kmol\,s$

k_{p1}, k_{p2}, k_{p3} reaction rate constant of propagation reaction, $m^3/kmol\,s$

$k_{L_{A0}}$ mass transfer coefficient for A_0 between bulk aqueous phase and polymer film, m/s

$k_{L_{B0}}$ mass transfer coefficient for B_0 between bulk organic phase and reaction zone, m/s

k_m phenomenological rate constant of nucleation, m^3/s

$K_{A0,ap}$ partition coefficient of A_0 between aqueous phase and polymer film

$K_{A0,ps}$ partition coefficient of A_0 between polymer film and organic solvent

$K_{A0,as}$ partition coefficient of A_0 between aqueous phase and organic phase

M_m molecular weight of P_m

M_{pN} instantaneous number-average molecular weight of precipitating polymer film

M_{pW} instantaneous weight-average molecular weight of precipitating polymer film

M_{sN} instantaneous number-average molecular weight of oligomers in solution

M_{sW} instantaneous weight-average molecular weight of oligomers in solution

$\bar{M}_{pN}$ time-averaged number average molecular weight of polymer film till time t

N_{CN} number of critical nuclei of polymer-rich phase formed due to phase separation by nucleation

P_{mr}	total concentration of oligomers of chain length m in the reaction zone ($=A_{mr}+B_{mr}+C_{mr}$)
R_{CN}	radius of critical nuclei of polymer-rich phase formed due to phase separation by nucleation, m
$S_{A\infty}$	total concentration of A type species in reaction zone, kmol/m^3
$S_{B\infty}$	total concentration of B type species in reaction zone, kmol/m^3
$S_{C\infty}$	total concentration of C type species in reaction zone, kmol/m^3
t	time, s
v_s	molar volume of organic solvent, m^3/kmol
V_a	aqueous-phase volume, m^3
V_s	organic-phase volume, m^3
V_m	volume of polymer-rich phase undergoing phase separation due to nucleation

Greek letters

ε	thickness of reaction zone, m
δ'	increase in the thickness of precipitated polymer film after one time integration step, m
δ_t	thickness of polymer film at any time t, m
δ_p	solubility parameter for Nylon 6–10 $(\text{cal/cm}^3)^{1/2}$
δ_s	solubility parameter for organic solvent $(\text{cal/cm}^3)^{1/2}$
ϕ_n	volume fraction of oligomer of chain length n
ϕ_p	volume fraction of polymeric species
ϕ_s	volume fraction of solvent
ρ_f	film density, kg/m^3
ρ_p	density of polymer, kg/m^3
χ	polymer–organic solvent interaction parameter

Superscripts

*	nondimensional quantity
0	initial condition
L	polymer-lean branch of the binodal curve
U	polymer-rich branch of the binodal curve

Subscripts

a	aqueous phase
CFM	chloroform
DCE	dichloro ethane
MC	methylene chloride
N	number-average molecular weight
n, m	chain length of oligomeric species
p	polymer film
r	reaction zone
s	organic solvent
W	weight average molecular weight

Overbar

(—)	averaged over time

REFERENCES

Brandrup, J. and Immergut, E.H. (1989) *Polymer Handbook*, Wiley, New York, U.S.A.

Cadotte, J., King, R., Majerle, R. and Petersen, R. (1981) Interfacial synthesis in the preparation of reverse osmosis membranes. *J. Macromol. Sci. Chem.* **A15**, 727.

Cheng, L. P., Dwan, A. H. and Gryte, C. C. (1995) *J. Polym. Sci. Part B*: *Polym. Phys.* **33**, 211–222.

Flory, P. J. (1953) *Principles of Polymer Chemistry*. Cornell University Press, Ithaca.

Fowkes, F. M. (1964) Attractive forces at interfaces. *Ind. Engng Chem.* **56**(12) 40–52.

Gonzalez–Ortiz, L. J. and Asua, J. M. (1996) Development of particle morphology in emulsion polymerization 3. Cluster nucleation and dynamics in polymerizing systems, *Macromolecules* **29**, 4520–4527.

Johnson, E. D. (1985) A study of the kinetics and mechanism of interfacial polymerization, Ph.D. dissestation. Carnegi-Mellom Univ., Pennsylvania.

Kamide, K., Ijima, H. and Matsuda, S. (1993) Thermodynamics of formation of porous polymeric membrane by phase separation method I. Nucleation and growth of nuclei. *Polym. J.* **25**(11), 1113–1131.

Karode, S. K. (1997) Studies in thin film composite membranes, Ph.D. dissertation. Indian Institute of Technology, Mumbai, India.

Karode, S. K., Kulkarni, S. S., Suresh, A. K. and Mashelkar, R. A. (1997), Molecular weight distribution in interfacial polymerization: model development and verification. *Chem. Engng Sci.* **52**(19), 3243–3255.

Khilar, K. C. (1987) *Encapsulation — A State of Art Report*. Department of Science and Technology. Government of India.

Morgan, P. W. (1965) *Condensation Polymers by Interfacial and Solution Methods*. Interscience, New York, U.S.A.

Morgan, P. W. and Kwolek, S. L. (1959) Interfacial polycondensation II. Fundamentals of polymer formation at liquid interfaces, *J. Polym. Sci.* **40**, 299. Owens, D. K. and Wendt, R. C. (1969) Estimation of the surface free energy of polymers, *J. Appl. Polym.* Sci. **13**, 1741–1747.

Petersen, R. J. (1993) Composite reverse osmosis and nanofiltration membranes, *J. Membrane Sci.* **83**, 81–150.

Press, W. H., Flannery, B. P., Teukolsky, S. A. and Vetterling, W. T. (1990) *Numerical Recipes*: *The Art of Scientific Computing* (*FORTRAN Version*). Cambridge University Press, Cambridge.

Yadav, S. K., Khilar, K. C. and Suresh, A. K. (1996) Microencapsulation in polyurea shell—Kinetics and film structure, *A.I.Ch.E. J.* **42**(9), 2616–2626.

Yadav, S. K., Suresh, A. K. and Khilar, K .C. (1990) Microencapsulation in polyurea shell by interfacial polycondensation, *A.I.Ch.E. J.* **36**(3), 431–438.